(Received 13 November 2024, Accepted 10 February 2025, Scheduled 19 February 2025)

Antenna Designs Using Kriging Assisted Taguchi Method

Jianing Ma[1], Xingning Jia[1,*], Ruidong Wang[2], and Liao Ma[1]

[1]School of Electronic and Electrical Engineering, Ningxia University, China
[2]School of Electrical Information Engineering, North Minzu University, China

ABSTRACT: Taguchi method has been extensively applied in electromagnetic optimization. To further enhance the optimization efficiency of the Taguchi method, a surrogate-assisted Taguchi method employing dynamic reduced rates is proposed. The reduced rate of each design variable is proportional to its contribution percentage. Variables with higher contributions exhibit a larger reduction rate, which subsequently decreases the search step and enhances the exploitation and convergence of the Taguchi method. Kriging model serves as a substitute for the real fitness evaluation in predicting the result of each experiment, with its feasible state determined by the average relative error of its predictions. This ensures the prediction accuracy while reducing the number of real fitness evaluations. The proposed algorithm is validated by the fact that the efficiency has increased at least twofold through four benchmark function tests. In the end, this algorithm is employed to synthesize the radiation pattern of an asymmetrical dipole array with 16 elements and to optimize the front-to-back ratio of the Yagi-Uda antenna.

1. INTRODUCTION

In recent years, surrogate-assisted evolutionary algorithms (SAEAs) have been widely employed in modern antenna design due to their high efficiency, robustness, and intelligence [1–3]. SAEAs generally consist of two components: surrogate model and evolutionary search engine, which work in a collaborative manner. The surrogate's prediction accuracy and evolutionary algorithm's search capability significantly influence its performance.

The Taguchi method (TM) is a global optimization algorithm that, by utilizing the orthogonal array (OA) and signal noise ratio (SNR), can achieve fast convergence and strong robustness without any gradient information. It has been widely used in filter designs [4], antenna array synthesis [5, 6], and other microwave design problems [7]. Nevertheless, the convergence of the TM is influenced by the reduced function, whose performance is sensitive to the reduced ratio. In addition, the original TM neglect accounting for the global optimal design from the conducting experiments established by the OA.

Since the performance of the TM is sensitive to the value of the reduced rate, an improved TM (ITM) based on the dynamic reduced rate is proposed, which only requires the specification of the reduced rate boundary [8]. In fact, some design parameters have a more significant impact on the design goal than others. Therefore, it is crucial to fine-tune these parameters during the optimization process to achieve optimal results. The relationship between the reduced rate and the contribution ratio of each parameter can be determined through the utilization of analysis of variance (ANOVA) on the experiment results. This is what we called a "dynamic reduced function" in ITM algorithm. Another method to improve the convergence of the TM involves substituting the costly computational model for a surrogate model. The experiments established by the OA during each iteration have a uniform distribution of parameters in the local design space. This means that training surrogate models like the Kriging model or artificial neural network on these experiment data can typically ensure lower prediction errors over this local design space.

In this paper, we present a surrogate-assisted TM (SATM) utilizing Kriging model to further enhance the local search capability and convergence efficiency of the ITM. The reduced rate of the level difference in the SATM is controlled by the dynamic reduced rate. The Kriging model serves as a substitute for the prohibitive computational model, thereby minimizing the number of real fitness evaluations. SATM is ultimately utilized in the synthesis of dipole antenna arrays and the design of Yagi-Uda antenna.

2. SATM ALGORITHM

The SATM is briefly based on the framework of the ITM algorithm, which involves the strategies of the dynamic reduced rate (DRR) and the optimal solution from the experiments established by the OA table. The DRR correlates with the contribution ratio of each factor, determined through ANOVA of the conducting experiments. A higher contribution ratio indicates a greater reduced rate and a smaller level difference. Moreover, the optimal result of the experiments is compared with the current global best obtained by the confirmation experiment to avoid the situation that the experiment result has met the termination criterion, yet the confirmation experiment remains unsatisfied. Besides, the Euclidean-based training data selection method is adopted to train the Kriging model. For each experimental parameter, non-repetitive samples closest to it are selected to ensure the prediction accuracy of the local surrogate model. The availability of the surrogate model is controlled by

* Corresponding author: Xingning Jia (nxujiaxn@nxu.edu.cn).

the average relative prediction error of the test samples. The SATM algorithm is described in the following detailed steps:

S0: Define the fitness function $f(\vec{x})$, where $\vec{x} = (x_1, \ldots, x_d)^T$ is a vector comprising design parameters. $x_i \in [x_i^L, x_i^U]$, where x_i^L and x_i^U denote the lower and upper boundaries of the factor x_i, $1 \leq i \leq d$, with d indicating the dimension of $\vec{x}$. Select the proper OA (M, K, S, 2) according to the value of d, where K is the factor number of the OA with the condition that $K \geq d$. S represents the level number, with a value of $S = 3$ in this paper. For the exponential reduced function, set the lower limit $r_{\min}$ and upper limit $r_{\max}$ of the reduced rate r. Initialize the global optimal value f_g and its corresponding design parameter $\vec{g}$; let e denote the average relative error of the prediction result of the surrogate model, with a threshold defined as $e_{\max}$. Initialize the surrogate model availability status $S_M = 0$. This indicates that the prediction accuracy of the surrogate model does not meet the requirements at this time, and only the real fitness function can be used to calculate $f(\vec{x})$. In other cases, the value $f(\vec{x})$ is estimated using the surrogate model. All parameters and results calculated by the real fitness function are stored in matrix **D** with dimensions of $q \times (k+1)$, which is an empty matrix in the initialization. Set the termination criterion and initialize the iteration count $t = 0$.

S1: Confirm the parameter values with respect to the different levels of each factor. Let the parameter values associated with levels 1, 2, and 3 of the factor x_i in the tth iteration be denoted as $x_i\ |_1^t$, $x_i\ |_2^t$, and $x_i\ |_3^t$. The relationship among them is outlined as follows: $x_i\ |_1^t = x_i\ |_2^t - L_i^t$, $x_i\ |_3^t = x_i\ |_2^t + L_i^t$, where L_i^t represents the level difference of factor x_i at the tth iteration. $L_i^t = r_i^t \times L_i^{t-1}$, where $1 \leq i \leq d$. Perform boundary checking, when $x_i\ |_1^t < x_i^L$, setting $x_i\ |_1^t = x_i^L$, and when $x_i\ |_3^t > x_i^U$, defining $x_i\ |_3^t = x_i^U$. In the initial iteration, to maximize coverage of the design space, the value for level 2, denoted as $x_i\ |_2^0$, is determined at the midpoint of the optimization range, calculated as $x_i\ |_2^0 = \left(x_i^U - x_i^L\right)/2$. The values for level 1 and level 3 are defined as $x_i\ |_1^0 = x_i\ |_2^0 - L_i^0$ and $x_i\ |_3^0 = x_i\ |_2^0 + L_i^0$, respectively, where $L_i^0 = \left(x_i^U - x_i^L\right)/(S+1)$.

S2: The vector $\vec{x}_n^t$ denotes the design parameter associated with the nth experiment in the tth iteration, where $1 \leq n \leq M$. The fitness value $f(\vec{x}_n^t)$ for each experiment is calculated. Calculate $f(\vec{x}_n^t)$ using the real fitness function under the conditions where $q \leq 3 \times M$ or $S_M = 0$. Subsequently, restore the parameter $\vec{x}_n^t$ and the result $f(\vec{x}_n^t)$ in the matrix **D**. In the event that the minimum value $f(\vec{x}_{n0}^t)$ within the set of values $f(\vec{x}_n^t)$ is less than the global best f_g, let $\vec{g} = \vec{x}_{n0}$ and proceed to S4. If $q \geq 3 \times M$ and $S_M = 0$, turn to S3 to construct the Kriging model. If $S_M = 1$, calculate the fitness values $\hat{f}(\vec{x}_n^t)$ for each experiment utilizing the Kriging model. Determine the minimum value within $\hat{f}(\vec{x}_n^t)$ represented as $\hat{f}(\vec{x}_{n0}^t)$, calculate $f(\vec{x}_{n0}^t)$ using the real fitness function if $\hat{f}(\vec{x}_{n0}^t) < f_g$, and restore the parameters $\vec{x}_{n0}^t$ and $f(\vec{x}_{n0}^t)$ in the matrix **D**. If $f(\vec{x}_{n0}^t) < f_g$, then set $\vec{g} = \vec{x}_{n0}$ and proceed to S4.

S3: Construct the Kriging model. Initialize the matrix **T** to be an empty matrix. If $q \geq 3 \times M$ and $S_M = 0$, calculate the Euclidean distances $|\vec{x}_n^t - \vec{D}_j|$ between every set of parameters $\vec{x}_n^t$ in the OA and the vector $\vec{D}_j$ in the matrix **D**. The top 20% samples closest to $\vec{x}_n^t$ are selected, duplicated, and subsequently recorded in matrix **T**. Suppose that the dimension of the current matrix **T** is $p \times (q+1)$, where $p \leq q$. The vectors in each row of matrix **T** are randomly arranged. The first $\lfloor 0.95p \rfloor$ rows are designated as the training dataset, while the subsequent $\lfloor 0.05p \rfloor$ rows are allocated for tests. The Kriging model is established based on the ooDACE toolbox [9]. For each test data $\vec{x}_i^c$ and its corresponding real fitness function value $f(\vec{x}_i^c)$, $1 \leq i \leq \lfloor 0.05p \rfloor$, the prediction values of the Kriging model are $\hat{f}(\vec{x}_i^c)$. The mean relative error e of all test data predictions $\hat{f}(\vec{x}_i^c)$ is calculated by (1). If $e \leq e_{\max}$, then $S_M = 1$.

$$e = \sum_{i=1}^{\lfloor 0.05p \rfloor} \frac{\left|\hat{f}(\vec{x}_i^c) - f(\vec{x}_i^c)\right|}{|f(\vec{x}_i^c)|} / \lfloor 0.05p \rfloor \tag{1}$$

S4: After obtaining the results of all experiments in the tth iteration, a response table is established through the analysis of mean (ANOM), and the elements of response table (RT) are determined by (2).

$$\eta_{k,s} = -10 \lg\left(\frac{1}{m}\sum_{i=1}^{m}\left(f_i^{k,s}\right)^2\right) \tag{2}$$

where $f_i^{k,s}$ represents the ith experiment value of factor k at level s. m is the total number of experiments in which the level of factor k is s. The value is converted to SNR. $\eta_{k,s}$ denotes the element value in RT corresponding to the level s of the Kth factor. For the minimization problem where the fitness function is positive, the criterion of "the larger the better" is applied. This indicates that the level value with the maximum value of each factor x_i in RT is the best level of the factor at present. The optimal level values of each factor are formed the confirmation experiment parameters, denoted as $\vec{x}_{opt}^t = (x_{o,1}^t, x_{o,2}^t, \ldots, x_{o,k}^t)$. Perform the confirmation experiment $f(\vec{x}_{opt}^t)$ and store the result in matrix **D**. If $f(\vec{x}_{opt}^t) < f_g$, then $\vec{g} = \vec{x}_{opt}$. ANOVA is performed on the experimental results from the tth iteration to determine the current contribution percentage P_i^t of each parameter, where $1 \leq i \leq d$, and the sum of all contribution percentages satisfies $\sum_{i=1}^{d} P_i^t = 1$. Then, the reduced rate r_i^{t+1}, which corresponds to the level difference L_i^t of factor x_i at the $t+1$ iteration, is calculated using Equation (3).

$$r_i^{t+1} = [r_{\max} - r_{\min}] \times P_i^t + r_{\min} \tag{3}$$

If $S_M = 0$, estimate $\hat{f}(\vec{x}_{opt}^t)$ using the Kriging model. Calculate the relative error e between $\hat{f}(\vec{x}_{opt}^t)$ and $f(\vec{x}_{opt}^t)$, and set $S_M = 0$ if $e \geq e_{\max}$.

S5: The termination criteria consist of the following conditions: the maximum number of real fitness evaluations

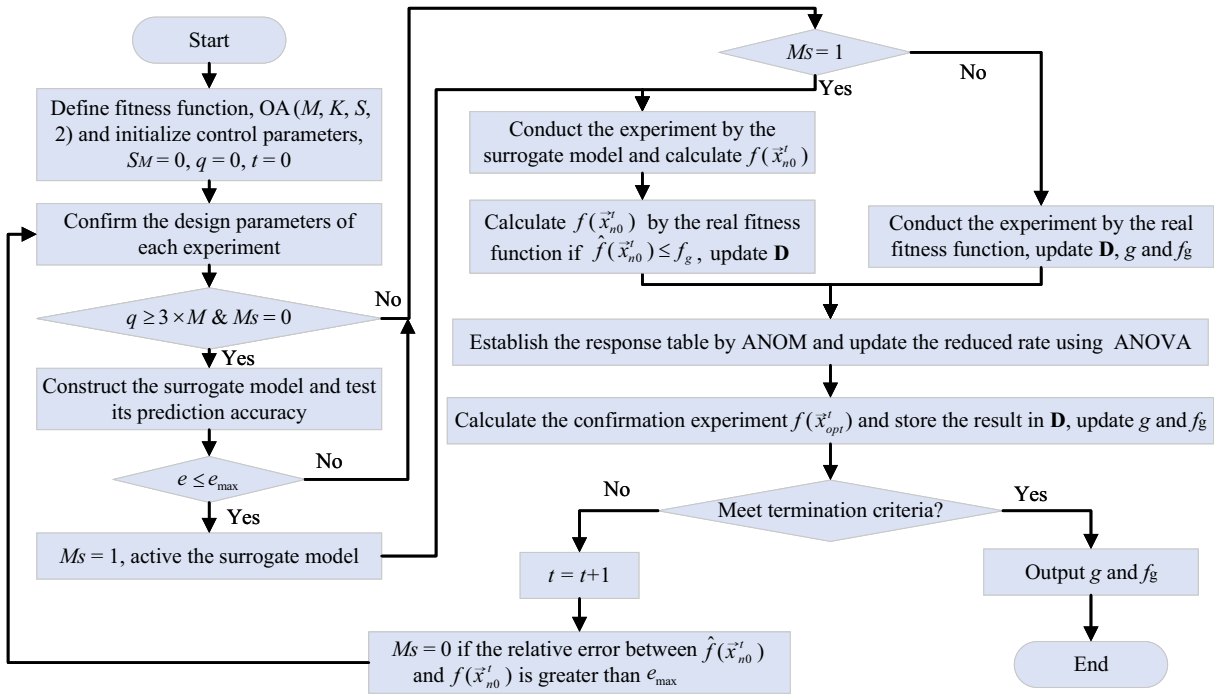

FIGURE 1. Flowchart of the proposed SATM algorithm.

TABLE 1. The value ranges of the benchmark functions and the parameter settings for the optimization algorithms.

Algorithms \ Benchmark	Fucntions	F1: Sphere	F2: Rastrigin	F3: Griewank	F4: Rosenbrock
	Boundaries	$-15 \le x_i \le 30$	$-4 \le x_i \le 5.12$	$-20 \le x_i \le 30$	$-20 \le x_i \le 30$
SATM		$e_{\max} = 0.05$ for F1	$e_{\max} = 0.05$ for F2	$e_{\max} = 0.01$ for F3	$e_{\max} = 0.03$ for F4
		OA (27, 13, 3, 2), $r_{\min} = 0.85$, $r_{\max} = 0.95$, MNRFEs = 1500			
ITM		OA (27, 13, 3, 2), $r_{\min} = 0.85$, $r_{\max} = 0.95$, $T_{\max} = 90$			
EO		$Np = 40$, $a_1 = 2$, $a_2 = 1$, $GP = 0.5$, $V = 1$, NRFEs = 2520			
TL-SSLPSO		$k = 3$, NRFEs = 1500			

(MNRFEs) must reach the predetermined value, or the function $f(\vec{g})$ must meet the specified value. If either condition is satisfied, return $\vec{g}$. Otherwise, $t = t + 1$, let $x_i\,|_2^{t+1} = x_{opt,i}^t$, and proceed to S1.

The flowchart of SATM algorithm is shown in Fig. 1.

3. EXPERIMENTAL STUDY

The Sphere, Rastrigin, Griewank, and Rosenbrock benchmark functions in 10 dimensions are selected for the purpose of comparing the performance of ITM and SATM algorithms. Table 1 presents the boundaries of each benchmark function, as well as the parameter settings for ITM and SATM algorithms. The first 10 columns of OA (27, 13, 3, 2) are selected, with $r_{\min} = 0.85$ and $r_{\max} = 0.95$, respectively. For the ITM algorithm, the maximum number of iterations is defined as $T_{\max} = 90$, which results in a total of 2520 real fitness evaluations. In SATM algorithm, MNRFEs are set to 1500. This study employs two additional algorithms for comparative analysis: equilibrium optimizer (EO) [10] and truncation-learning-driven surrogate assisted social learning particle swarm optimizer (TL-SSLPSO) [11]. These algorithms represent recent advancements in the fields of meta-heuristic and surrogate-assisted evolutionary optimization methods. The control parameter settings for EO and TL-SSLPSO are also provided in Table 1.

Figure 2 shows the convergence curves for the four benchmark functions optimized by ITM, SATM, EO, and TL-SSLPSO algorithms, respectively. It can be seen from Figs. 2(a)–(c) that, in comparison to the results of ITM algorithm, the prediction performance of the Kriging model of SATM algorithm meets the requirements when $t = 7$. The optimization results of SATM algorithm demonstrate significant improvements over ITM algorithm when being evaluated with the same number of real fitness evaluations (NRFEs). TL-SSLPSO shows faster convergence when being applied to the sphere function; however, it encounters local minima in the other two functions. For the Rosenbrock function, the Kriging model of SATM algorithm achieves the required prediction accuracy at $t = 24$. The optimal result, with respect to meeting

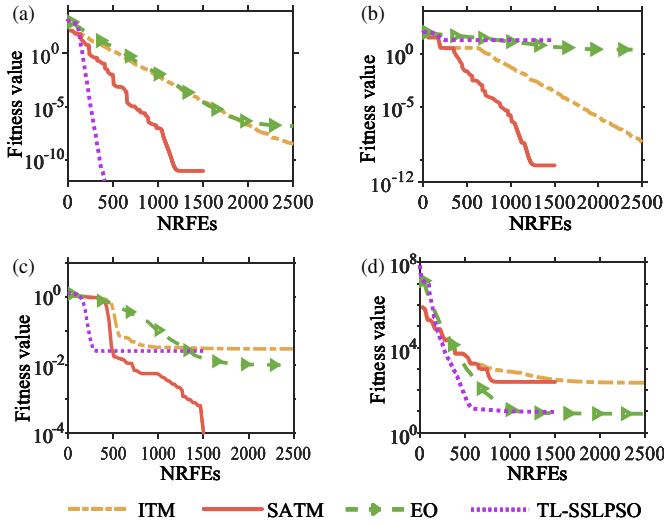

FIGURE 2. Convergence curves of ITM, SATM, EO and TL-SSLPSO for the (a) Sphere, (b) Rastrigin, (c) Griewank and (d) Rosenbrock benchmark functions.

the termination condition, is nearly identical to the result generated by the ITM algorithm. The local prediction accuracy of Kriging for the Rosenbrock function is inferior, resulting in convergence at a local optimum. However, the results of SATM algorithm are better than those of the ITM algorithm under the same NRFEs. Moreover, the results obtained by EO and TL-SSLPSO are significantly lower than those achieved by ITM and SATM. Overall, SATM algorithm can achieve the same optimization results with an average of 50% fewer real fitness evaluations than ITM algorithm.

4. DIPOLE ARRAY SYNTHESIS

By optimizing the relative position, excitation amplitude, and phase of the array elements, the antenna array synthesis based on intelligent optimization algorithm can realize the controllable adjustment of the direction pattern, which is useful in the fields of communication, remote sensing, radar, and other fields [12]. The synthesis of dipole arrays for low-RCS [13] and shaped patterns [14, 15] has been investigated using optimization methods. In this section, as illustrated in Fig. 3, an asymmetric 16-element half-wave dipole array is placed horizontally along the z-axis, where the array spacing is $\lambda_0/2 \approx 2$ m, and λ_0 represents the wavelength operating at 75 MHz in free space. The dipole element is a rectangular metal sheet that is fed at the center of the dipoles. The Method of Moment (MOM) is employed to compute the radiation characteristics of a half-wave dipole array [16]. According to MOM's discretization requirements, each dipole cell is divided into 48 grids, so the entire array is divided into 768 grids in total. It is required to synthesize low sidelobe level and null control by optimizing the excitation magnitudes for each element, with the excitation magnitude values ranging from 0 to 1. In order to compare the performance of the proposed algorithm, the convergence results for ITM, EO, and TL-SSLPSO are also given. ITM and SATM algorithms utilize first 16 columns of OA (54, 25, 3, 2). The control parameters for SATM algorithm are defined as follows: $r_{\min} = 0.85$, $r_{\max} = 0.95$, and $e_{\max} = 0.02$.

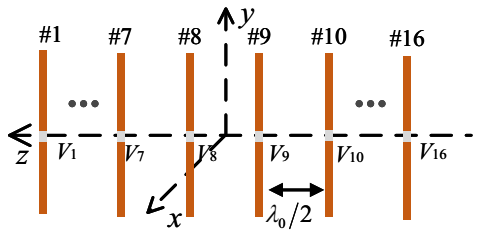

FIGURE 3. Configuration of the 16-element dipole array.

4.1. Null Control

In this example, by optimizing the excitation magnitudes of each dipole, three radiation pattern cases with low sidelobe and nulls in specified directions are investigated. At XOZ plane, all three array patterns exhibit a low sidelobe level that falls within the range of $[-25\,\text{dB}, -20\,\text{dB}]$. In case 1, the nulls occur in the narrow directions of $\theta = [44°, 53°]$ and $[128°, 137°]$, whereas in case 2, they are located in the wide directions of $\theta = [40°, 60°]$ and $[120°, 140°]$. In case 3, the nulls are found in the asymmetry directions of $\theta = [35°, 55°]$ and $[120°, 145°]$. The fitness function for this example is defined in (4), with AF_{UB} and AF_{LB} denoting the upper and lower limits of the constrained values of the array radiation pattern, as depicted by the black dashed lines in Figs. 4(e)–(g), respectively, $d\theta = 0.9°$ in this case. Hence, the optimal value of the fitness function is 0. The termination condition for ITM and SATM algorithms is defined by two criteria: either reaching the maximum number of iterations, specified as $T_{\max} = 50$, or achieving a global best value of 0.

4.2. Sidelobe Suppression

In this example, the optimization goal is to suppress the sidelobe level of the array pattern through the adjustment of the dipole's excitation magnitude. The termination condition of the algorithm is the maximum number of iterations $T_{\max} = 50$.

4.3. Results and Discussions

The parameter settings for EO and TL-SSLPSO are consistent with those utilized in benchmark optimizations. The fitness value statistics from ten independent runs for SATM, EO, and TL-SSLPSO algorithms are detailed in Table 2. SATM yields the lowest best and average values for cases 1 and 2 of the null control. In contrast, TL-SSLPSO achieves the lowest best and average values for case 3 of the null control and sidelobe suppression. The optimal values achieved by ITM algorithm are greater than those obtained by SATM, as well as the average values, demonstrating that SATM has superior search abilities relative to ITM algorithm.

$$f = \int_{0°}^{180°} [\text{AF}(\theta) - \text{AF}_{\text{UB}}(\theta)] \left[\frac{1 + \text{sgn}(\text{AF}(\theta) - \text{AF}_{\text{UB}}(\theta))}{2}\right] d\theta$$

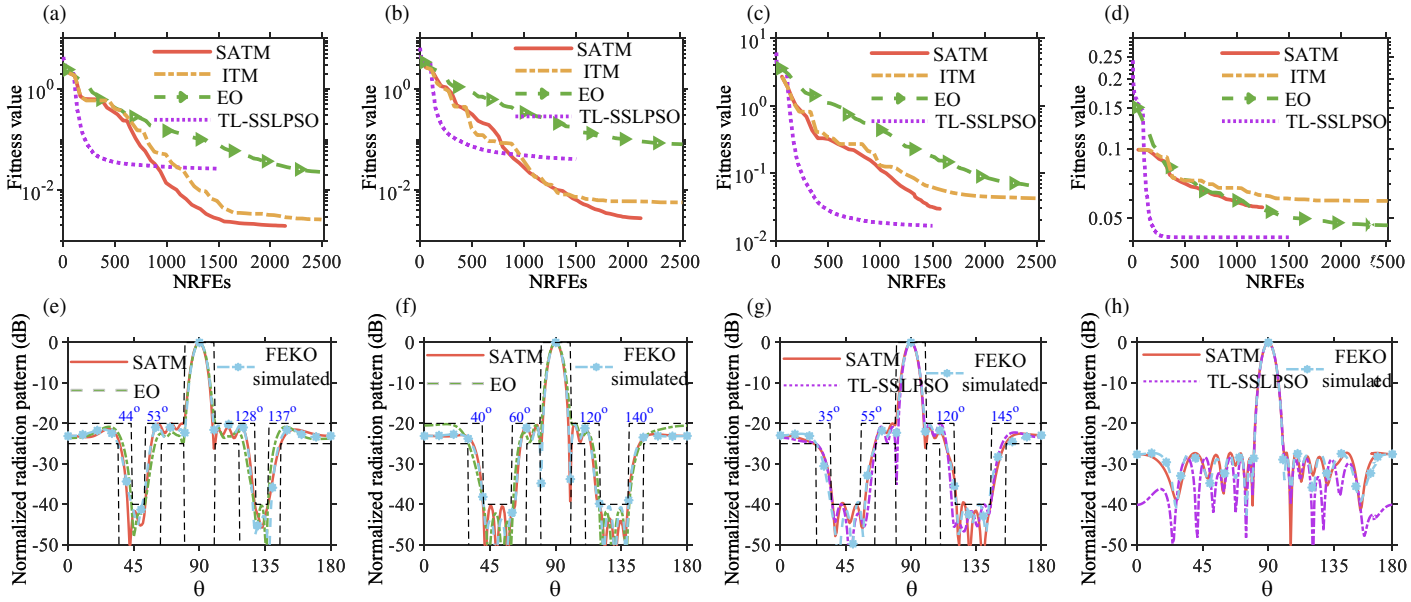

FIGURE 4. Convergence curves and the two optimal normalized radiation patterns obtained from SATM, ITM, EO, and TL-SSLPSO for null control (a), (e) case 1, (b), (f) case 2, (c), (g) case 3, and (d), (h) sidelobe level suppression, respectively.

TABLE 2. Statistics of dipole array synthesis

Cases		Algorithms	SATM	ITM	EO	TL-SSLPSO
Null Control	Case 1	Worst	5.11E-03	2.52E-03	6.05E-02	4.71E-02
		Best	**0**		**0**	6.05E-02
		Average	**2.03E-03**		2.24E-02	2.65E-02
	Case 2	Worst	1.04E-02	5.62E-03	1.65E-01	1.47E-01
		Best	**0**		2.29E-04	4.83E-03
		Average	**3.71E-03**		7.29E-02	4.08E-02
	Case 3	Worst	4.35E-02	4.19E-02	1.25E-01	3.98E-02
		Best	1.35E-02		9.42E-03	**2.84E-03**
		Average	2.96E-02		5.88E-02	**1.66E-02**
Sidelobe Suppression		Worst	6.25E-02	5.94E-02	5.19E-02	4.92E-02
		Best	4.34E-02		4.14E-02	**3.81E-02**
		Mean	5.57E-02		4.62E-02	**4.14E-02**

$$+\int_{0^\circ}^{180^\circ}[\mathrm{AF_{LB}}(\theta)-\mathrm{AF}(\theta)]\left[\frac{1+\mathrm{sgn}(\mathrm{AF_{LB}}(\theta)-\mathrm{AF}(\theta))}{2}\right]d\theta \tag{4}$$

Figures 4(a)–(c) present the convergence curves for null control cases derived from SATM, ITM, EO, and TL-SSLPSO. SATM exhibits the lowest average fitness values for case 1 and case 2 with almost a 22% reduction in NRFEs relative to ITM algorithm. Figs. 4(e)–(f) illustrates the optimal normalized radiation patterns for case 1 and case 2, as derived from SATM and EO algorithms. In the asymmetry null control case, i.e., case 3, as depicted in Fig. 4(c), TL-SSLPSO exhibits superior performance compared to the other three algorithms. Therefore, the optimal radiation patterns achieved by TL-SSLPSO and SATM are depicted in Fig. 4(g). In the sidelobe suppression case shown in Fig. 4(d), upon reaching the maximum number of iterations, the optimal values achieved by SATM and ITM are 0.0434 (-27.25 dB) and 0.0594 (-24.52 dB), respectively. SATM algorithm requires a total of 1246 real fitness evaluations, which means a decrease of 54.7% with respect to the NRFEs performed by ITM algorithm. The average and optimal values achieved by SATM are comparable to those obtained by EO and higher than those achieved by TL-SSLPSO. Fig. 4(h) presents the optimal radiation patterns obtained by SATM and TL-SSLPSO. Moreover, the radiation patterns associated with the optimal results achieved by SATM are simulated using the commercial electromagnetic software FEKO (computations involving bodies of arbitrary shape) [17], and these patterns coincide with the MOM simulations performed in MATLAB [16].

5. YAGI-UDA ANTENNA DESIGN

A Yagi-Uda antenna (YUA), which is usually used as an example for verifying the performance of optimization algorithm, is

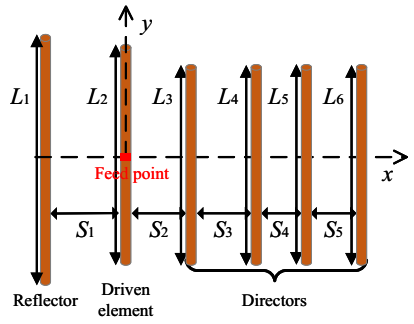

FIGURE 5. Configuration of the six-element Yagi-Uda antenna ($0.15\lambda_0 \leq S_j \leq 0.45\lambda_0, j = 1, 2, \cdots, 5, 0.42\lambda_0 \leq L_i \leq 0.52\lambda_0$, $i = 1, 2, 0.4\lambda_0 \leq L_i \leq 0.495\lambda_0, i = 3, 4, 5, 6$).

adopted in this section [18, 19]. The configuration of YUA, illustrated in Fig. 5, comprises a driven element, a reflector, and four directors. All elements are circular metal posts with lengths denoted as L_i $(i = 1, 2, \ldots, 6)$. The space distance between adjacent posts is represented as S_j, where $j = 1, 2, \ldots, 6$. It is known from [20] that the best directivity of a six-element YUA is 13.41 dB without accounting for the front-to-back ratio (FBR). The objective is to ensure that the directivity D exceeds 13.41 dB, in addition to achieving a higher FBR. The objective function is defined as (5).

$$\text{Minimize } F = \gamma \max\{0, 13.41 - D\} - FBR + 50 \quad (5)$$

$$FBR = 20\log_{10}\{E(\theta = 90°, \phi = 0°) / \max[E(\theta = 90°, \phi_b)]\} \quad (6)$$

where the first term in (5) is a plenty function, ensuring that the directivity D is not less than 13.41 dB in this case. The FBR is calculated by (6), which denotes the ratio of the electric field at a point $(\theta = 90°, \phi = 0°)$ to the maximum electric field at the points $(\theta = 90°, \phi_b \in [160°, 200°])$. γ is set to 10^3 in this case to ensure that the directivity criterion is met firstly, then to maximize the FBR during the optimization. The constant 50 is added here to make the minimum value of F be greater than 0.

OA (27, 13, 3, 2) is selected for the YUA design, with parameters set as follows: $r_{\min} = 0.85$ and $r_{\max} = 0.95$ for ITM and SATM, respectively, and $e_{\max} = 0.05$ for SATM. The MNRFEs are set to 10^3. In this case, the YUA is modeled using FEKO, comprising dipoles of a designated length with radius of $0.003369\lambda_0$, where λ_0 denotes the wavelength operating at 165 MHz in free space. The statistics for each algorithm applied to YUA designs are presented in Table 3.

TABLE 3. Statistics of YUA design.

Algorithms	SATM	ITM	EO	TL-SSLPSO
Worst	25.15		656	692.55
Best	23.94	25.15	28.87	**22.47**
Average	**24.51**		398.48	438.41
Success rate	**100%**	**100%**	40%	20%

Despite the TL-SSLPSO achieving the best fitness value, it reached the desired directivity only once in five independent runs. SATM demonstrates a lower average fitness value and greater robustness in this case. The convergence curves for ITM, SATM, EO, and TL-SSLPSO are shown in Fig. 6(a). It is obvious that the Kriging model first substitutes the real fitness evaluation after 10 iterations. After 366 NRFEs, the minimum value achieved by SATM is 23.94, which is 1.21 less than the minimum value obtained by ITM, resulting in a reduction of NRFEs by nearly 20%. The directivity and FBR achieved through SATM are 13.42 dB and 26.06 dB, respectively. The FBR achieved by SATM exhibits superiority compared to that obtained through ITM, as proven by the normalized directivity displayed in Fig. 6(b). This demonstrates the capability of SATM to enhance the optimization efficiency of ITM. An optimum YUA, as described in [20], is shown in Fig. 6(b), without considerations for FBR optimization, which has a value of 10.05 dB. The directivity of this YUA is 13.58 dB; however, its FBR is 16 dB lower than the optimal result obtained by SATM.

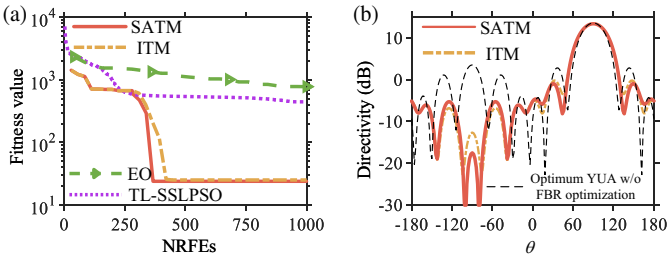

FIGURE 6. (a) Convergence curves of ITM, SATM, EO and TLSSLPSO for the YUA design and (b) directivity patterns simulated by FEKO, corresponding to the optimal results achieved by ITM, SATM, and the optimum array without FBR optimization [20], respectively.

6. CONCLUSION

SATM algorithm, which is based on the Kriging model and dynamic reduced function, is proposed to enhance the optimization efficiency of TM. This algorithm is applied to benchmark functions, dipole array synthesis, and Yagi-Uda antenna problems. The benchmark function experiments indicate that SATM algorithm exhibits greater efficiency and enhanced optimization capabilities relative to ITM algorithm. The proposed algorithm has a good potential for the application in high computational cost design problems.

ACKNOWLEDGEMENT

This work was supported in part by the National Natural Science Foundation of China under Grant 62461051, in part by the Nature Science Foundation of Ningxia Hui Autonomous Region under Grant 2024AAC03046, in part by the Key Research and Development Program of Ningxia Hui Autonomous Region under Grant 2021BEB04068, and in part by the 2024 Central Government Guided Local Science and Technology Development Special Project (Ningxia Hui Autonomous Region) under Grant 2024FRD05054.

REFERENCES

[1] Peng, F. and X. Chen, "An efficient optimization method for antenna arrays using a small population diploid genetic algorithm based on local RBF networks," *IEEE Transactions on Antennas and Propagation*, Vol. 72, No. 4, 3237–3249, 2024.

[2] Wu, Q., Y. Cao, H. Wang, and W. Hong, "Machine-learning-assisted optimization and its application to antenna designs: Opportunities and challenges," *China Communications*, Vol. 17, No. 4, 152–164, 2020.

[3] Fu, K., X. Cai, B. Yuan, Y. Yang, and X. Yao, "An efficient surrogate assisted particle swarm optimization for antenna synthesis," *IEEE Transactions on Antennas and Propagation*, Vol. 70, No. 7, 4977–4984, 2022.

[4] Sahu, S., J. Ali, P. Yupapin, and G. Singh, "Effectiveness of taguchi method for the optimization of narrowband optical filters based on grating waveguides," *Microsystem Technologies*, Vol. 25, 789–795, 2019.

[5] Amara, W., R. Kheder, R. Ghayoula, I. E. Gmati, A. Smida, J. Fattahi, and L. Latrach, "Taguchi method-based synthesis of a circular antenna array for enhanced IoT applications," *Telecom*, Vol. 6, No. 1, 7, 2025.

[6] Xu, X., C. Liao, Y. Cheng, and F. Peng, "An improved Taguchi algorithm based on fitting and prediction for linear antenna array synthesis," *International Journal of Antennas and Propagation*, Vol. 2019, No. 1, 7351521, 2019.

[7] Zhang, L., D. Lu, S. Yang, Y. Chen, and B. Li, "Design of a quint-band passive NGDC by using Taguchi's optimization method," *AEU — International Journal of Electronics and Communications*, Vol. 171, 154921, 2023.

[8] Jia, X. and G. Lu, "An improved Taguchi's method for electromagnetic applications," *Progress In Electromagnetics Research Letters*, Vol. 87, 89–96, 2019.

[9] Gorissen, D., I. Couckuyt, P. Demeester, T. Dhaene, and K. Crombecq, "A surrogate modeling and adaptive sampling toolbox for computer based design," *Journal of Machine Learning Research*, Vol. 11, 2051–2055, 2010.

[10] Faramarzi, A., M. Heidarinejad, B. Stephens, and S. Mirjalili, "Equilibrium optimizer: A novel optimization algorithm," *Knowledge-Based Systems*, Vol. 191, 105190, 2020.

[11] Yu, H., L. Kang, Y. Tan, C. Sun, and J. Zeng, "Truncation-learning-driven surrogate assisted social learning particle swarm optimization for computationally expensive problem," *Applied Soft Computing*, Vol. 97, 106812, 2020.

[12] Li, M., Y. Liu, and Y. J. Guo, "Shaped power pattern synthesis of a linear dipole array by element rotation and phase optimization using dynamic differential evolution," *IEEE Antennas and Wireless Propagation Letters*, Vol. 17, No. 4, 697–701, 2018.

[13] Wang, W.-T., S.-X. Gong, Y.-J. Zhang, F.-T. Zha, J. Ling, and T. Wan, "Low RCS dipole array synthesis based on MoM-PSO hybrid algorithm," *Progress In Electromagnetics Research*, Vol. 94, 119–132, 2009.

[14] Liu, F., Y. Liu, K. D. Xu, Y.-L. Ban, Q. H. Liu, and Y. J. Guo, "Synthesizing uniform amplitude sparse dipole arrays with shaped patterns by joint optimization of element positions, rotations and phases," *IEEE Transactions on Antennas and Propagation*, Vol. 67, No. 9, 6017–6028, 2019.

[15] Li, M., Y. Liu, and Y. J. Guo, "Design of sum and difference patterns by optimizing element rotations and positions for linear dipole array," *IEEE Transactions on Antennas and Propagation*, Vol. 69, No. 5, 3027–3032, 2020.

[16] Makarov, S. N., V. Iyer, S. Kulkarni, and S. R. Best, *Antenna and EM Modeling with MATLAB Antenna Toolbox*, John Wiley & Sons, 2021.

[17] "FEKO Suite 7.0 — Field computations involving bodies of arbitrary shape," Altair Development S.A. (Pty) Ltd., Stellenbosch, South Africa, May 2014, http://www.feko.info.

[18] Baumgartner, P., T. Bauernfeind, O. Bíró, A. Hackl, C. Magele, W. Renhart, and R. Torchio, "Multi-objective optimization of Yagi-Uda antenna applying enhanced firefly algorithm with adaptive cost function," *IEEE Transactions on Magnetics*, Vol. 54, No. 3, 1–4, 2017.

[19] Nouri, M., H. Behroozi, A. Jafarieh, S. A. Aghdam, M. J. Piran, and N. K. Mallat, "A learning-based dipole Yagi-Uda antenna and phased array antenna for mmWave precoding and V2V communication in 5G systems," *IEEE Transactions on Vehicular Technology*, Vol. 72, No. 3, 2789–2803, 2022.

[20] Balanis, C. A., *Antenna Theory: Analysis and Design*, John Wiley & Sons, 2016.